Cell

Structure and Mechanism of a Metal-Sensing Regulatory RNA

Charles E. Dann III,[1,2] Catherine A. Wakeman,[1,2] Cecelia L. Sieling,[1] Stephanie C. Baker,[1] Irnov Irnov,[1] and Wade C. Winkler[1,*]

[1]Department of Biochemistry, The University of Texas Southwestern Medical Center, Dallas, TX, 75390, USA

[2]These authors contributed equally to this work.

*Correspondence: wade.winkler@utsouthwestern.edu

DOI 10.1016/j.cell.2007.06.051

SUMMARY

Organisms maintain the correct balance of intracellular metals primarily through metal-sensing proteins that control transport and storage of the target ion(s). Here, we reveal the basis of metal sensing and genetic control by a metalloregulatory RNA. Our data demonstrate that a previously uncharacterized orphan riboswitch, renamed the "M-box," is a divalent metal-sensing RNA involved in Mg^{2+} homeostasis. A combination of genetic, biochemical, and biophysical techniques demonstrate that Mg^{2+} induces a compacted tertiary architecture for M-box RNAs that regulates the accessibility of nucleotides involved in genetic control. Molecular details are provided by crystallographic structure determination of a Mg^{2+}-bound M-box RNA. Given the distribution of this RNA element, it may constitute a common mode for bacterial metal ion regulation, and its discovery suggests the possibility of additional RNA-based metal sensors in modern and primordial organisms.

INTRODUCTION

Metal ions are a requirement for life but become an intracellular threat when present in excess. Studies from many laboratories have revealed how homeostasis mechanisms are elegantly controlled for a variety of metals (Moore and Helmann, 2005; Pennella and Giedroc, 2005). Despite these advancements, relatively little detail is known regarding Mg^{2+} homeostasis even though Mg^{2+} is the most abundant divalent metal within cells and is required for numerous biochemical activities. Historically, proteins have been shown to fulfill metalloregulatory roles in organisms, but the extent to which these functions should be solely ascribed to proteins has not been determined.

Biological roles for RNAs have expanded rapidly in recent years and recent data suggest that RNA can adopt discrete structures that efficiently regulate gene expression. These RNAs, commonly known as riboswitches, are widespread structures that become conformationally altered in response to metabolic or stress cues in order to control gene expression (reviewed in Batey, 2006; Winkler and Breaker, 2005; Winkler, 2005a). Riboswitches typically are composed of two portions: a conserved aptamer domain that senses metabolic signals followed by sequence elements that control transcription termination (e.g., Mironov et al., 2002), translation initiation efficiency (e.g., Winkler et al., 2002), or mRNA stability (e.g., Winkler et al., 2004), in response to ligand binding. As a reflection of their importance for overall genetic circuitry, more than 70 *cis*-acting regulatory RNAs have been identified in *Bacillus subtilis* that respond to proteins, tRNAs, or metabolites (Winkler, 2005b). Recently, it was suggested that the 5′ untranslated region (5′ UTR) of a *Salmonella enterica* Mg^{2+} transport gene employs a cation-responsive riboswitch (Cromie et al., 2006). However, the exact basis for metal ion recognition and the mechanism of metal-induced genetic control have not been elucidated for this interesting RNA. Folding studies have established clearly that RNAs use divalent ions to stabilize tertiary interactions (Draper et al., 2005; Woodson, 2005). Thus, RNA-based divalent metal ion sensors would be expected to carefully couple metal-induced RNA folding with genetic control. Herein we describe an RNA element, coined the M-box, that fulfills these criteria. Our studies of this regulatory RNA class reveal the underlying logic for an RNA-based equivalent to metalloregulatory proteins.

RESULTS

Mg^{2+}-Specific Regulation of *B. subtilis mgtE*

Bioinformatics-aided efforts have uncovered several RNA elements that share traits with established riboswitches but whose metabolic signals remain to be identified (Barrick et al., 2004; Corbino et al., 2005). Typically, the ligand binding domain (aptamer) of a riboswitch is evolutionarily conserved while the remaining portions exhibit significant sequence diversity and participate in genetic control processes. Herein we designate the aptamer domain for one orphan riboswitch class, originally termed the *ykoK* element, as the "M-box." This structural motif is generally located upstream of Mg^{2+} transport genes in Gram-positive bacteria (Figure S1 in the Supplemental Data available with this article online) (Barrick et al., 2004; Griffiths-Jones et al., 2005). Mg^{2+} transport in bacteria is achieved

primarily through the use of three protein families: CorA, MgtE, and MgtA/MgtB P-type ATPase proteins (Gardner, 2003; Hmiel et al., 1986; Kehres and Maguire, 2002; Maccdiarmid and Gardner, 1998; Maguire, 2006; Smith and Maguire, 1995, 1998). Depending on the organism, M-box RNAs can be found in UTRs of all three classes of transport genes, although they are primarily co-transcribed with members of the *mgtA* and *mgtE* families. Although M-box RNAs are usually coupled with transport proteins, the RNA element in also localized with genes of unknown function (Barrick et al., 2004; Figure S1).

B. subtilis contains at least one homolog for all three Mg^{2+} transporter classes, although only the *mgtE* homolog is preceded by the M-box RNA (Figure S1). Specifically, the *B. subtilis* genome contains two candidate *corA* genes (*yfjQ, yqxL*), a candidate *mgtA* gene (*yloB*), and one *mgtE* homolog (*ykoK*). Under Mg^{2+}-limited conditions, transcript abundance of *mgtE* was significantly increased while *corA* and *mgtA* transcript levels were not appreciably changed (data not shown). Manual inspection of the *mgtE* locus revealed a candidate promoter element that was confirmed by 5′ mapping and fusion to a *lacZ* reporter (Figures 1E and S2). Together, these data indicated that the *mgtE* mRNA contains a 409 nucleotide 5′ UTR that encompasses the M-box RNA element.

To investigate the basis of its regulation, the 5′ UTR of *mgtE* was fused to *lacZ* and ectopically integrated into the genome. Cells were cultured under 'normal' defined minimal medium conditions (*i.e.* adequate metal concentrations) except that a different divalent ion was selectively depleted during each experiment (Figures 1B–1D). Expression of *lacZ* was substantially increased in response to Mg^{2+} deprivation, but not upon depletion of Mn^{2+} or Fe^{2+}. As a correlative experiment, cells were depleted for all divalent ions and *lacZ* expression levels were measured upon supplementation of individual metals (Figure 1F). Only the addition of Mg^{2+} repressed *lacZ* expression under these conditions. Together, these data demonstrated that *mgtE-lacZ* expression is selectively repressed by Mg^{2+} in vivo. This regulatory response did not occur at the level of transcription initiation as expression of a promoter-*lacZ* construct is unchanged with varying Mg^{2+} (Figure 1E). To rule out the possibility that Mg^{2+}-responsive regulation was due to RNA structural defects in general, we also tested *lacZ* fusions to unrelated RNAs. In contrast to *mgtE*, Mg^{2+} limitation did not increase expression of either *S*-adenosylmethionine- or glucosamine-6-phosphate-sensing RNAs (Figure 1E).

Transcription Attenuation In Vivo

Inspection of the *mgtE* 5′ UTR revealed the presence of a candidate intrinsic transcription terminator, an observation supported by reverse transcriptase stop experiments and structural probing data (Figures 1A, 2, 3F, and S2). The 5′ portion of the terminator helix appeared to be capable of pairing with the 3′ portion of a helix (P1) within the M-box domain, thereby forming an antiterminator. Most other members of this regulatory RNA class were also found to contain candidate terminator and antiterminator elements (Figure S1 and unpublished data) (Barrick et al., 2004; Griffiths-Jones et al., 2005). Together, these observations suggest that M-box RNAs control expression of downstream genes via regulated terminator formation, a mechanism commonly referred to as transcription attenuation (Landick and Yanofsky, 1987).

As a preliminary test of this mechanism, the aptamer domain was fused to *lacZ*, thereby deleting the downstream terminator region. Expression was increased ~6.5-fold relative to the full-length sequence, reflecting the loss of the termination signal (Figure 1E). This construct also exhibited a loss of Mg^{2+}-induced repression, demonstrating that the terminator helix is required for regulation. Similarly, site-specific mutation of the terminator (M5) also led to an increase (~5-fold) in Mg^{2+}-independent expression. In contrast, compensatory mutations designed to restore the terminator helix but disrupt the antiterminator (M6) decreased overall expression and diminished responsiveness to Mg^{2+}. The M6 mutant's partial responsiveness to Mg^{2+} is due to the lack of disruption in the 5′ portion of antiterminator helix. Together, these mutational analyses demonstrate that interruption of the interplay between terminator and antiterminator elements deleteriously impacts Mg^{2+}-responsive regulation of *mgtE* in vivo.

To test whether structural integrity of the aptamer domain was required for Mg^{2+} repression, mutations were introduced (M1-M4) into this region (Figure 1A). M1 was altered within a nonconserved portion of the P5 helix and reduced Mg^{2+} repression to 2.2- from 7.5-fold (Figure 1E). Compensatory mutations designed to restore this helix (M2) partially restored Mg^{2+} repression, supporting the P5 pairing as predicted by sequence analyses. M3 was altered at a highly conserved portion of P5 and exhibited almost complete elimination of Mg^{2+}-induced repression. A similar loss in Mg^{2+}-responsiveness resulted from alteration of a conserved side-bulge within P2 (M4). Together, these data are consistent with our expectations that the aptamer region functions as a sensory domain for an intracellular metabolic signal and regulates expression via transcription attenuation.

Mg^{2+}-Induced Transcription Termination In Vitro

The recapitulation of transcription attenuation mechanisms in vitro has been accomplished for a variety of metabolite-sensing RNAs (e.g., Mironov et al., 2002; reviewed in Winkler and Breaker, 2005). These experiments typically include only RNA polymerase, ribonucleotides, and DNA templates that encompass the regulatory RNA. A specific effect upon termination through addition of a metabolite is taken as strong evidence that accessory protein factors are not required for attenuation. We therefore measured the effect of Mg^{2+} on transcription termination within the *mgtE* 5′ UTR in vitro. These reactions result in transcription run-off products and transcripts truncated at the terminator helix (Figure 2A). Data collected at several Mg^{2+} concentrations reveal an increase in termination in response to Mg^{2+}, albeit a modest ~15% overall (Figure 2B).

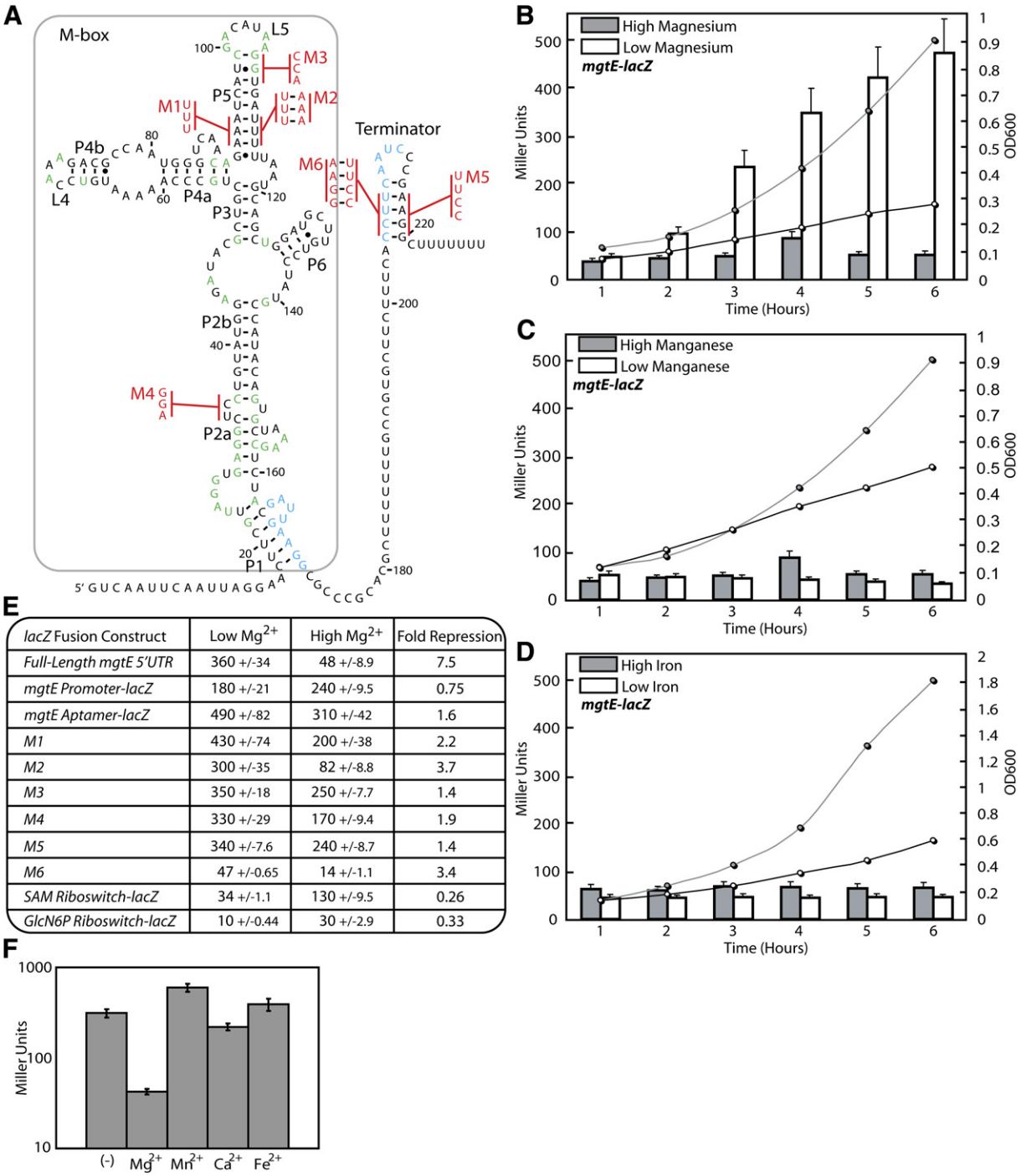

E

lacZ Fusion Construct	Low Mg^{2+}	High Mg^{2+}	Fold Repression
Full-Length mgtE 5′UTR	360 +/-34	48 +/-8.9	7.5
mgtE Promoter-lacZ	180 +/-21	240 +/-9.5	0.75
mgtE Aptamer-lacZ	490 +/-82	310 +/-42	1.6
M1	430 +/-74	200 +/-38	2.2
M2	300 +/-35	82 +/-8.8	3.7
M3	350 +/-18	250 +/-7.7	1.4
M4	330 +/-29	170 +/-9.4	1.9
M5	340 +/-7.6	240 +/-8.7	1.4
M6	47 +/-0.65	14 +/-1.1	3.4
SAM Riboswitch-lacZ	34 +/-1.1	130 +/-9.5	0.26
GlcN6P Riboswitch-lacZ	10 +/-0.44	30 +/-2.9	0.33

Figure 1. Magnesium-Responsive Regulation of *B. subtilis mgtE* In Vivo

(A) Secondary structure of the 5′ portion (nucleotides +1 to 228) of *B. subtilis mgtE* (Figure S1). Green nucleotides match the consensus pattern for positions that are conserved at 95% or greater. The AUG start codon for *mgtE* begins 180 nucleotides downstream of the terminator. Site-directed mutations are denoted in red letters. Cyan indicates the putative antiterminator pairing. The boxed region denotes the M-box, the aptamer domain, of the regulatory RNA.

(B–D) Nucleotides −486 to + 25 relative to the translational start were fused to *lacZ*. Line plots reflect OD_{600} measurements and correspond to the right-side *y* axis (shaded and open circles indicate conditions of 'high' and 'low' metals). Bar graphs reflect expression of the *lacZ* reporter fusion (Miller Units) (filled and open bars indicate conditions of "high" and "low" metals). Cells were cultured to mid-exponential phase whereupon they were pelleted, washed, and resuspended to OD_{600} = 0.1 in medium containing "high" or "low" extracellular metal concentrations. Aliquots were removed for analysis at hourly intervals.

Typically, intrinsic terminators consist of a G+C-enriched helix followed by a polyuridine tract (de Hoon et al., 2005; Gusarov and Nudler, 1999). Unique within the current members of its riboswitch class and rare compared to all intrinsic terminators, the *mgtE* regulatory RNA has an unpaired nucleotide between its terminator helix and polyuridine stretch (C221). Deletion of C221 improved the dynamic range for Mg^{2+}-induced termination in vitro to ~40% overall (Figure 2C). Furthermore, transcription termination by the M3 mutant was unresponsive to Mg^{2+} levels, indicating that aptamer integrity was required for termination (Figure 2B). As a control for aptamer-independent effects of Mg^{2+} on termination, the *mgtE* promoter was fused immediately upstream of the terminator helix. Increased Mg^{2+} had little effect on termination for this construct, demonstrating that the terminator alone is not stabilized by Mg^{2+} (Figure 2C). To further validate transcription attenuation as the general genetic control mechanism for M-box RNAs, the region upstream of *B. cereus bc4140* (*mgtA*) was assayed under these conditions (Figure 2D). This M-box RNA exhibited Mg^{2+}-induced termination with a dynamic range of ~70%. In contrast, varying Mg^{2+} had no effect on termination for an established *S*-adenosylmethionine (SAM)-responsive transcription attenuator. Therefore, M-box RNAs are direct divalent metal sensors that promote transcription attenuation in the absence of accessory proteins.

Mg^{2+} Induces a Compacted Conformation

To determine the impact of Mg^{2+} on RNA structure, we employed several structural probing methods (Figures 3 and S3–S8). Specifically, we interrogated *mgtE* M-box RNAs via selective 2′-hydroxyl acylation analyzed by primer extension (SHAPE) (Merino et al., 2005). This assay measures the relative rates of reactivity of *N*-methylisatoic anhydride (NMIA) to 2′-hydroxyls, a reaction influenced by internucleotide flexibility. However, SHAPE is a recently described method that has not been examined over a wide range of divalent concentrations. Therefore, *mgtE* RNAs were also analyzed by in-line probing, which measures the relative rate of spontaneous scission at internucleotide linkages. Previous experiments demonstrate that proper in-line configuration between the 2′-hydroxyl and the 5′-oxyanion leaving group is the predominant feature dictating these cleavage rates (Li and Breaker, 1999; Soukup and Breaker, 1999). However, it is likely that nucleophilicity of the 2′-hydroxyl is also influenced at high metal ion concentrations. It was therefore important to apply both techniques to verify that data obtained by either method were consistent and not the result of a heretofore unrecognized Mg^{2+}-specific artifact introduced by each respective technique.

These reactions included the M-box domain alone (nucleotides 14-172, relative to the transcriptional start site) or 'full-length' RNAs, which completely encompass the aptamer and terminator regions (nucleotides 1-265 and 1-220 for SHAPE and in-line probing, respectively). Regions of NMIA reactivity (SHAPE) and spontaneous cleavage (in-line probing) largely agreed with the secondary structure as predicted by comparative sequence analyses, with bands primarily corresponding to unpaired nucleotides. Addition of Mg^{2+} leads to lowered reactivity, indicating greater structural constraint, for over 40 internucleotide linkages (Figures 3A, 3B, 3D–3F, and S3–S5). Each individual change in reactivity occurred at similar Mg^{2+} concentrations, suggesting that the change in RNA conformation was concerted with an EC_{50} of ~0.6 mM and ~2.7 mM Mg^{2+} for aptamer and full-length RNAs, respectively (Figures 3D and 3E). Furthermore, Mg^{2+}-specific changes in the aptamer acted in concert with altered reactivity of terminator and antiterminator positions (Figure 3F). Importantly, these latter probing changes agreed well with the predicted switching between antiterminator and terminator base-pairing schemes (Figure 3F inset). For example, positions 211-213 exhibited increased NMIA reactivity upon exposure to the high Mg^{2+} conformation, consistent with their relocation from the antiterminator helix to the terminator terminal loop. The data therefore provide biochemical evidence that Mg^{2+}-induced aptamer changes are responsible for downstream terminator formation. Probing of the M3 mutant, which exhibited a loss of Mg^{2+}-induced transcription attenuation in vivo and in vitro, revealed that structural features within the L5 terminal loop were acutely disrupted while the remaining structure appeared to be similar to wild-type RNA in low [Mg^{2+}] (Figure 3F inset and Figure S7). However, despite the close overall structural resemblance to wild-type RNAs, M3 RNAs were incapable of the Mg^{2+}-induced conformational change, suggesting a direct role for L5 in the Mg^{2+}-folded state.

mgtE RNAs were also subjected to footprinting by hydroxyl radicals, which measures cleavage of the solvent accessible backbone in a manner independent of sequence or secondary structure (Latham and Cech, 1989). This test enriched the SHAPE and in-line probing data by directly assessing whether the Mg^{2+}-induced conformational change correlates with formation of a closely packed internal core, a feature of sophisticated RNA tertiary structures. Footprinting of the aptamer domain in the presence of 20 μM or 20 mM Mg^{2+} revealed an array of Mg^{2+}-induced protections within internal and terminal loops (Figures 3C and 3F), demonstrating that indeed a solvent inaccessible core was formed in the presence of Mg^{2+}. From these probing data, a model emerges wherein

(E) Variants of the *mgtE-lacZ* fusion were tested for expression with 2.5 mM or 0.005 mM Mg^{2+}. All experiments were repeated at least in triplicate. Construction of the *B. subtilis yitJ-lacZ* (SAM riboswitch) and *glmS-lacZ* (glucosamine-6-phosphate riboswitch) fusions are described elsewhere (Winkler et al., 2003, 2004).

(F) *B. subtilis* strains containing the *mgtE-lacZ* fusion were grown in minimal media containing either no divalent ions or the indicated ion at 50 μM. Under these conditions, only the addition of Mg^{2+} caused specific reduction in β-galactosidase activity.

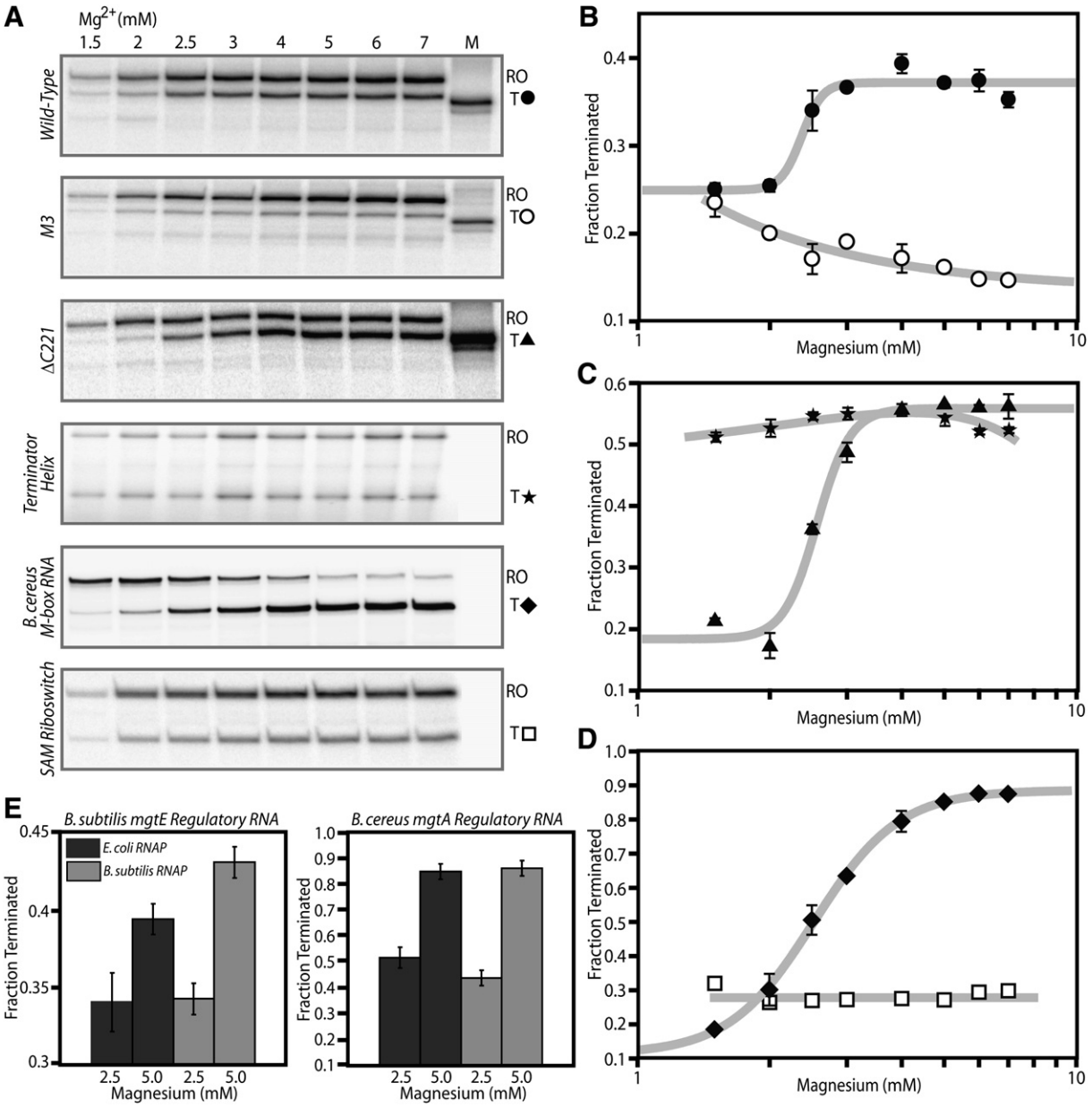

Figure 2. Mg^{2+} Induces Transcription Termination In Vitro

Bacterial RNA polymerase and NTPs were incubated with PCR-generated DNA templates. Mg^{2+} concentration was varied and transcript products were resolved by denaturing 6% PAGE.

(A) Transcription assays using templates encompassing wild-type, M3, ΔC221, or terminator sequences from the *B. subtilis mgtE* 5′ UTR, a *B. cereus* M-box RNA, and a *B. subtilis S*-adenosylmethionine (SAM) riboswitch at multiple [Mg^{2+}]. Lower and upper bands correspond to termination at the intrinsic terminator (T) or run-off transcription (RO), respectively. A size marker for transcripts containing a 3′ terminus at the base of the terminator helix is shown in the last lane of the first three panels. Only M-box RNAs with an intact aptamer and terminator show Mg^{2+}-dependent transcription termination. Mg^{2+} levels do not affect the termination of M3, terminator alone, or the unrelated SAM riboswitch transcript. The *mgtE* promoter (Figure S2) was fused immediately upstream of the terminator for the terminator-alone template.

(B–D) The fraction termination is shown plotted against Mg^{2+} concentration for wild-type (closed circles), M3 control (open circles), ΔC221 (triangles), terminator alone (stars), *B. cereus* M-box RNA (diamonds), and a *B. subtilis* SAM riboswitch (open squares).

(E) Representative assays were conducted using *B. subtilis* and *E. coli* RNA polymerase with DNA templates for *B. subtilis mgtE* and *B. cereus mgtA* (*bc*4140). These reactions confirmed that similar termination control was exhibited by different bacterial polymerases.

the aptamer domain is dominated by secondary structure in the presence of low or no Mg^{2+} but is substantially rearranged upon Mg^{2+} association to include higher order tertiary structure.

To investigate whether Mg^{2+} are specifically required for tertiary structure formation, probing tests were repeated in the presence of high (2 M) monovalent ions (Figure S3; data not shown). Under these conditions monovalents are expected to outcompete the loosely-associated divalent ion atmosphere, leaving only high-affinity divalent sites (Das et al., 2005; Draper et al., 2005). Probing patterns were similar between the two conditions (2.1 M and 0.1 M monovalent ions), indicating that divalent ions are specifically required for the tertiary conformation. Furthermore, EC_{50} values for the Mg^{2+}-induced conformational change were similar between the two conditions (data not shown). Therefore, although monovalent ions induce tertiary structure formation for certain RNAs (Takamoto et al., 2004), divalent ions are specifically required for M-box tertiary structure. To investigate whether similar effects may be observed for riboswitches in general, unrelated metabolite-sensing RNAs were also subjected to probing assays (Figure S6). Probing of a flavin mononucleotide-sensing RNA revealed Mg^{2+}-induced structural changes under the low monovalent ion conditions. However, this effect was abolished upon an increase in monovalents. Further testing of SAM and thiamine pyrophosphate riboswitches revealed that they too exhibited a lack of Mg^{2+}-responsive structural changes under high monovalent conditions. These data both contrast and highlight the specific requirement for Mg^{2+} in folding of the *mgtE* M-box RNA. Additionally, we conducted probing reactions in the presence of cobalt hexammine, a fully hydrated Mg^{2+} mimic that can substitute at Mg^{2+} sites when only outer-shell RNA-metal contacts are required (Cowan, 1993) (data not shown). M-box RNAs were not conformationally modified by increasing cobalt hexammine and the resulting probing patterns closely resembled those obtained under low Mg^{2+} conditions, suggesting that inner-sphere Mg^{2+} coordination is required for tertiary structure formation.

To directly measure whether the RNA undergoes a significant change in overall shape in its ligand-bound form, wild-type and M3 aptamer RNAs were subjected to analytical ultracentrifugation (AUC) (Figures 4A, 4B, and S8). During conditions of low (30 μM) or high (10 mM) Mg^{2+}, single RNA species were observed that displayed a sedimentation coefficient of 5.6 and 7.0, respectively, revealing that association of Mg^{2+} was indeed accompanied by a significant decrease in hydrodynamic radius. Mg^{2+}-induced compaction was highly cooperative with a Hill coefficient of 4.29 ± 0.88 and exhibited an EC_{50} of 0.16 mM, a value that approximately correlated with the structural probing results (Figures 4B and S8). In contrast, the M3 mutant demonstrated a sedimentation coefficient of 5.9 even in the presence of 10 mM Mg^{2+}, confirming that it was incapable of forming the compacted structure and was confined to a secondary structure-dominated state. Based on these data, we reasoned that the extended and compacted conformations might be separated by size exclusion chromatography. Indeed, aptamer RNA equilibrated in 30 μM Mg^{2+} eluted at an earlier retention time relative to 10 mM Mg^{2+} (Figures 4C and S8). However, M3 RNAs equilibrated in 10 mM Mg^{2+} exhibited a retention time nearly identical to wild-type RNAs that had been equilibrated in 30 μM Mg^{2+}. This result supports the hypothesis that M3 RNA is a reliable control for the extended conformational state. Therefore, we exploited these observations for comparison of the retention times for M3 and wild-type RNAs equilibrated in divalent metals other than Mg^{2+}. These tests revealed that divalent ions other than Mg^{2+} can also elicit the compacted tertiary conformation (Figure 4C). Preliminary in-line probing confirmed that at least one of these alternative metals, Ca^{2+}, induced a structural rearrangement identical to Mg^{2+}, although potential differences in EC_{50} values for the remaining divalent ions were not assessed (data not shown). Additionally, SHAPE probing of M-box RNAs in the presence of 5 mM Ca^{2+} or Mn^{2+} revealed that alternative divalent ions could induce terminator helix formation similar to Mg^{2+} (Figure 4D). Together these data indicated that the M-box RNA structure is likely to be a general sensor for divalent metals in vitro, although the compacted tertiary conformation is specifically tuned to in vivo Mg^{2+} levels.

Three-Dimensional Model of Mg^{2+}-Bound M-box RNA

Our genetic, chemical probing, and biophysical analyses of the *mgtE* UTR strongly support a role for this RNA as a direct Mg^{2+} sensor, but these data would benefit greatly from a visualization of the mechanism of metal sensing. To this end, we determined the crystal structure of the M-box domain from *mgtE* at 2.6 Å with a refined model R_{free} of 24.6% (Figures 5–7 and S10–S13; Table S1). Three-dimensional structures have been determined for several metabolite-sensing RNAs, offering a preview of the architectural features that might be expected for M-box RNAs (Batey, 2006). In addition, multiple RNAs have structures that employ specific metal binding sites, hinting at mechanisms that could be used for metal sensing. For example, specific Mg^{2+} sites have been identified for thiamine pyrophosphate-binding RNAs, group I introns, and the ribosome, wherein the metal ions participate in ligand stabilization, chemical catalysis, and structural stabilization, respectively (DeRose, 2003; Hougland et al., 2005; Klein et al., 2004; Selmer et al., 2006; Serganov et al., 2006; Vicens and Cech, 2006). These different structures stabilize Mg^{2+} through at least one inner-sphere contact, most often via the nonbridging oxygen of a phosphate group, although they also interact with nucleobase functional groups and ribose oxygens. The fact that partially dehydrated Mg^{2+} are also required by M-box RNAs suggested they will share similar features with these other sites.

RNA crystals were grown in the presence of 10 mM Mg^{2+}, a concentration that resulted in a structure in the ligand-bound state. The RNA adopts a complex

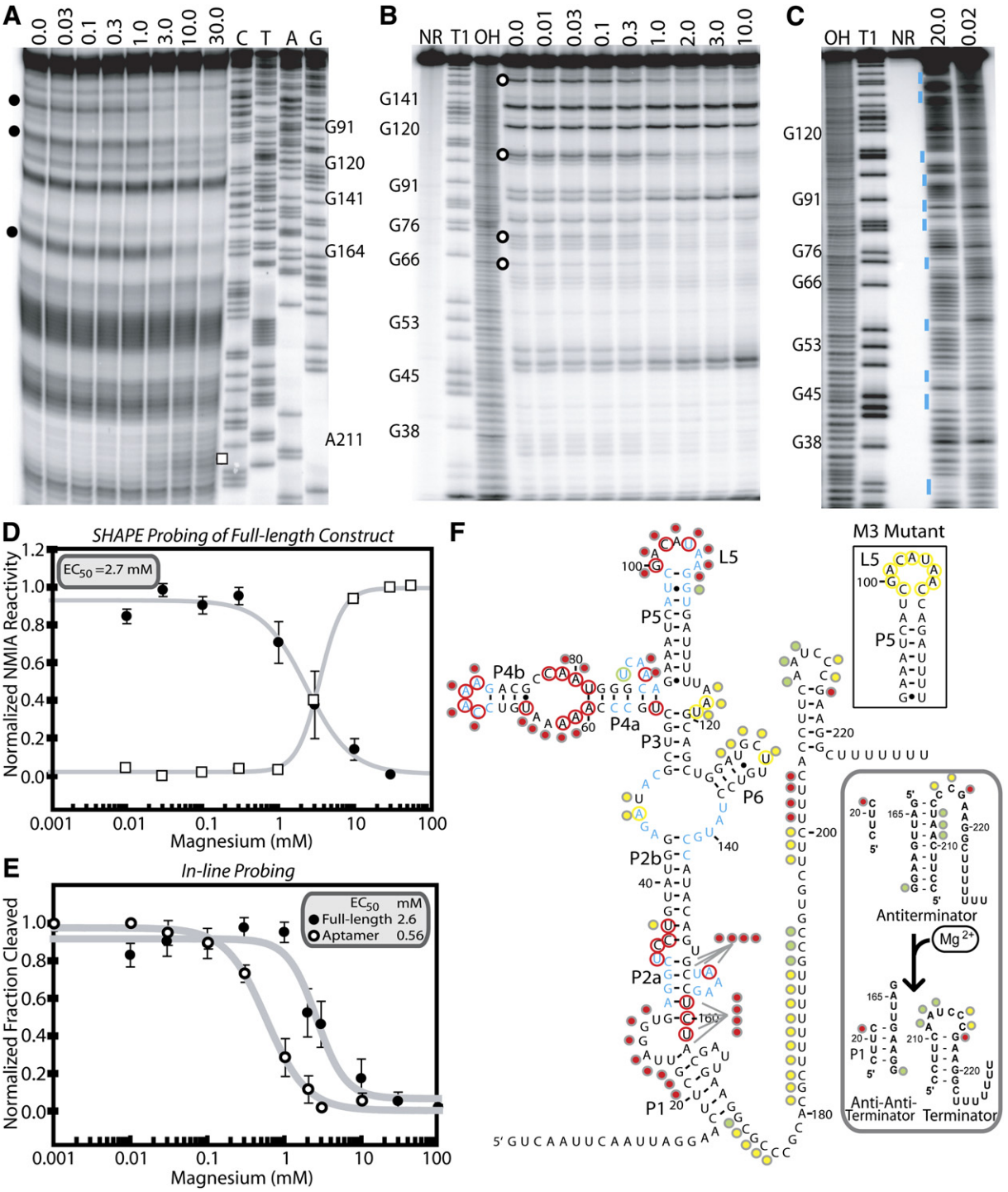

Figure 3. Association of Mg^{2+} Leads to a Conformational Change

(A) Representative SHAPE probing of the *mgtE* regulatory RNA (nucleotides 1–265) incubated with increasing [Mg^{2+}] (as indicated in mM), adjacent to DNA sequencing ladders. Reactions contained 2.1 M monovalent ions to outcompete loosely associated divalent ions. Examples of SHAPE probing of the aptamer domain alone or with lowered monovalent ions are included in Figure S3. Filled circles and the open square in panel (A) indicate representative positions that decrease or increase in NMIA reactivity, respectively.

(B) Representative in-line probing of the aptamer region (nucleotides 14–172) incubated with increasing [Mg^{2+}] (as indicated in mM), adjacent to control lanes (NR, nonreacted RNA; OH, hydroxyl-mediated cleavage at all positions; T1, cleavage at G). Reactions contained 2.1 M monovalent ions. Additional examples of in-line probing reactions for aptamer and full-length RNAs are included in Figures S4–S7. Open circles in panel (B) indicate representative positions that decrease in spontaneous scission in response to increased Mg^{2+}.

three-dimensional architecture, mostly comprising three closely packed, nearly parallel helices. The P3 helix forms a coaxial stack with P4, which folds alongside P2 and P5. The secondary structure of the aptamer agrees well with that based on covariation and conservation, but significant changes are seen in the P2 region (cf. Figures 1A and 5A). In total, the structure agrees well with the chemical probing data, including the positioning of hydroxyl radical protections within a closely packed internal core (Figure 5E). Additionally, the majority of positions that demonstrated decreased internucleotide flexibility in response to Mg^{2+} (Figure 3F) are located at a region where the three parallel helices converge via a network of long-range contacts. A most exciting aspect of the structural model involves the presence of six Mg^{2+} that also reside predominantly in this region of tertiary contacts (Figures 5, 6, S10, and S11). Extensive inner- and outer-sphere contacts to Mg^{2+}, with coordination distances of 2.1 to 2.2 Å and 2.6 −3.2 Å, respectively, occur for nucleotides in the P2, L4, and L5 regions of the RNA (Figures 6A and S10). Mg^{2+} mediate multiple long-range interactions, leading to stabilization of the compact three-helical tertiary structure. Together, the chemical probing data, measurements of changes in hydrodynamic radius, and the tertiary structure combine to suggest a model wherein the extended P4 and P5 helices clamp against P2 to form the compacted three parallel helix structure in response to binding of Mg^{2+}.

In addition to the Mg^{2+}, four potassium ions (K^+) are also modeled in the structure. To assess the role of K^+ in the tertiary structure of the RNA, probing assays were repeated in the presence or absence of Mg^{2+} and a range of monovalent concentrations (Figure S9). These tests revealed that the Mg^{2+}-bound conformation could be induced even in the absence of monovalent ions. Furthermore, sedimentation velocity measurements of Mg^{2+}-associated RNAs were identical in the absence or presence of K^+ (Figure 4A). In contrast, the presence of high monovalent ions in the absence of Mg^{2+} did not result in formation of the compact tertiary conformation (Figure S3–S5). Therefore, tertiary folding of M-box RNAs is strictly dependent upon divalent ions, despite the presence of four K^+ in the structural model.

Of the six Mg^{2+}, Mg1 exhibits the most inner-shell RNA contacts, consisting of three contacts to L5 nonbridging phosphate oxygens (G100, C102, and A103) and a contact to U104 O4 (Figures 6, S10, and S11). These interactions ultimately engender a sharp change in backbone directionality to the looped residues. The same Mg^{2+} mediates multiple outer-shell RNA contacts to L5 positions through two associated waters. Although there is precedence for RNA-bound Mg^{2+} with four inner-sphere RNA contacts (Type IV) they are rare in published structures (Cate et al., 1997; Klein et al., 2004). The low incidence of type IV Mg^{2+} in RNA structures and the fact that Mg1 organizes the L5 structure for docking with P2 and L4 indicate that Mg1 likely constitutes a key component in establishing the tertiary architecture. Mg2 also appears to be important for the tertiary conformation as it coordinates nonbridging phosphate oxygens of G100 (L5) and U23 (P2), acting to bring the parallel P5-P2 helices together (Figures 6A, 6B, and S11). A third Mg^{2+}, Mg3, helps position the P2 noncanonical A25-C160 pair and the highly conserved U24 position, which flips out to stack together with A155, a base that is itself flipped out from the P2 helix as a result of a near-classical UAA/GAN motif (Figure 6A, 6B, and S11) (Lee et al., 2006). As a result of the Mg3-stabilized local structure, both U24 and A155 can form long-range base interactions to L5 positions. Many long range pairing interactions within the RNA structure involve residues within L5 and P2; therefore, given the intimate involvement of Mg^{2+} (Mg1-3) with these regions, they are likely to comprise the key metals for the tertiary conformation and metal sensing. However, Mg4 may also be important as it contacts the L4 tetraloop structure, which also mediates several long-range base interactions to P2 and L5 (Figures 6A and S11). Interestingly, despite its sequence, CAAA, the L4 tetraloop superimposes well with a common RNA tertiary interaction motif, the GNRA tetraloop (Figure S12). The two remaining Mg^{2+} associate to the modestly conserved P4 internal loop (Figures 6A and S11).

(C) Hydroxyl radical footprinting of the aptamer domain in the presence of 0.02 mM or 20.0 mM Mg^{2+}. Vertical blue bars indicate regions of Mg^{2+}-induced protection against hydroxyl radicals. NR, T1, and OH identify no reaction, partial digestion with nuclease T1, and partial digestion with alkali, respectively.

(D) Filled circles and the open square in panel (A) indicate representative positions that decrease or increase in NMIA reactivity, respectively. The decreasing reactivity for positions corresponding to 69–72, 97–100, and 159–163 was normalized, graphed, and subjected to curve-fitting analysis. The increase in reactivity for positions 211–213 was normalized and graphed alongside this composite curve. These data indicate an EC_{50} value of ~2.7 mM for the construct that included the entire regulatory region (nucleotides +1 to +265), including the terminator.

(E) Open circles in panel (B) indicate representative positions that decrease in spontaneous scission in response to increased Mg^{2+}. The decreasing reactivity for positions corresponding to 65, 72, 104, and 154 was normalized, graphed, and subjected to curve-fitting analysis. These data indicate an EC_{50} value of 0.56 mM for the aptamer alone (nucleotides 14–172). Additional in-line probing (shown in Figure S5) revealed an EC_{50} of ~2.6 mM for constructs that incorporated the entire regulatory region (nucleotides +1 to +220).

(F) Summary of hydroxyl radical, SHAPE and in-line probing data overlayed with the *mgtE* RNA sequence. Positions of Mg^{2+}-induced protection against hydroxyl radical cleavage are indicated in blue letters. Red, green, and yellow circles positioned adjacent to nucleotides denote internucleotide linkages that decrease, increase, or remain unchanged in their overall reactivity to NMIA (SHAPE) in response to increased Mg^{2+}, respectively. Red, green, and yellow circles that encircle nucleotides denote internucleotide linkages that exhibit decreased, increased, or unchanged spontaneous cleavage in response to increased Mg^{2+}, respectively. Hydroxyl radical footprinting, in-line probing, and SHAPE data could be interpreted for positions 29–161, 29–161, and 20–230, respectively. The probing pattern for M3 RNAs was identical to wild-type in low [Mg^{2+}] (Figure S7), except for disruption of L5, as shown in the inset. The second inset highlights the agreement between SHAPE probing data and the helical regions postulated to be involved in genetic control (antiterminator, terminator, P1).

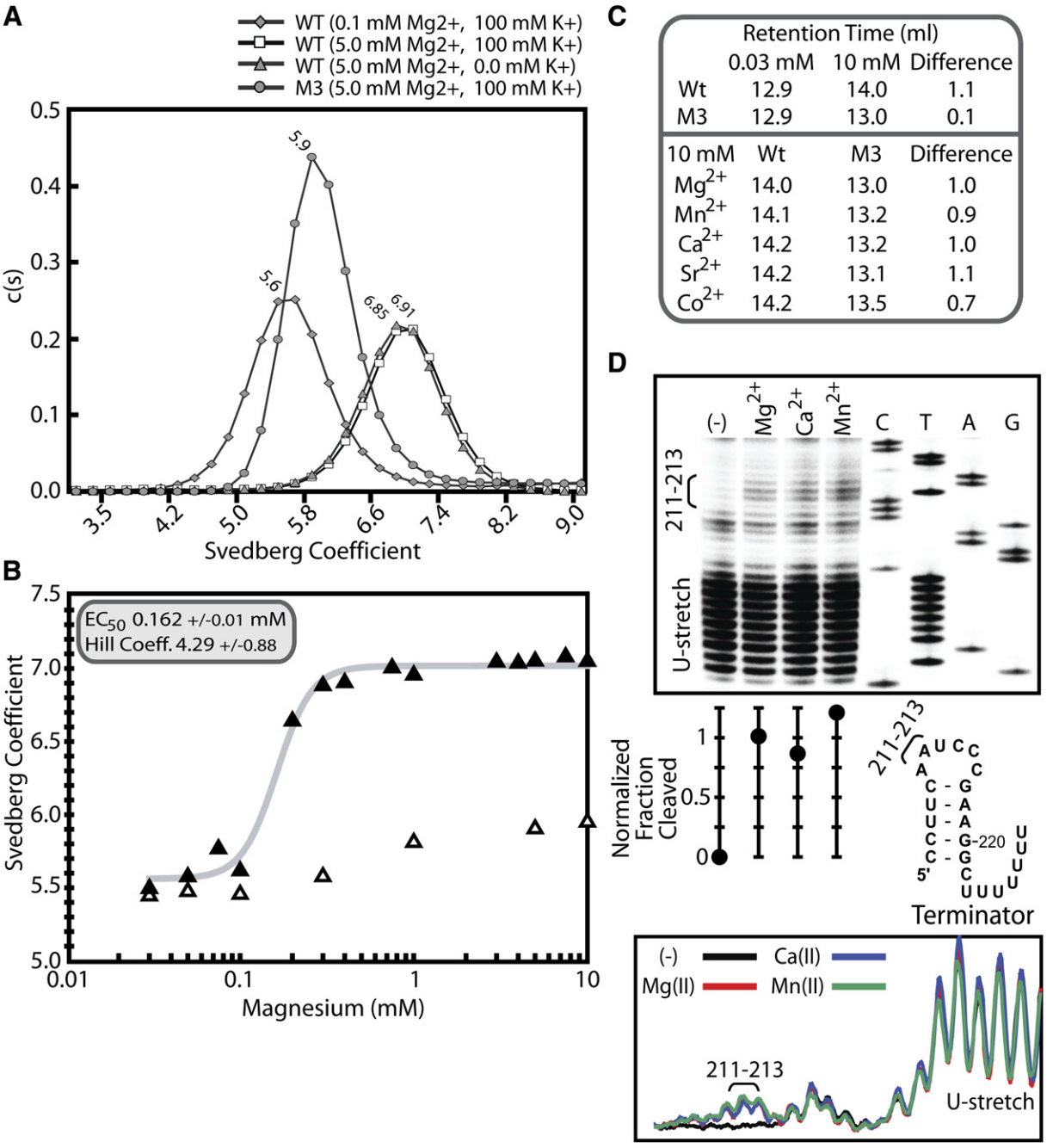

Figure 4. Mg^{2+}-Induced Compaction of M-box RNAs

(A) Wild-type and M3 RNAs were subjected to analytical ultracentrifugation (AUC) in the presence of high and low Mg^{2+} (wild-type in 5 mM Mg^{2+} = open squares; wild-type in 0.1 mM Mg^{2+} = filled diamonds; wild-type in 5 mM Mg^{2+} and absence of potassium = filled triangles; M3 in 5 mM Mg^{2+} = filled circles). Wild-type aptamer RNA exhibited a change in sedimentation coefficient when equilibrated in high Mg^{2+} relative to low Mg^{2+}. However, M3 RNAs demonstrated a sedimentation coefficient most similar to low Mg^{2+} conditions, despite the presence of increased Mg^{2+}. When 100 mM KCl was added alongside 10 mM Mg^{2+}, the RNA exhibited the same sedimentation coefficients as a reaction lacking KCl, indicating that potassium ions are dispensable for Mg^{2+}-induced tertiary formation.

(B) AUC of wild-type aptamer RNAs (filled triangles) revealed a highly cooperative change in sedimentation velocity in response to Mg^{2+}. In contrast, M3 RNAs (open triangles) underwent a considerably smaller change in hydrodynamic radius under identical conditions. Additional parameters are shown in Figure S8.

(C) Given that M3 RNA serves as a control for the low-[Mg^{2+}], extended conformation, retention times were compared for wild-type and M3 RNAs equilibrated in alternate divalent metals. These data suggest that alternate divalent ions can also induce the compacted conformation.

The multiple long range base interactions in the structure occur predominately between L4, L5, P2, and J2/1, regions in proximity to both Mg^{2+} and antiterminator nucleotides (Figures 5A, 7, S12, and S13). A common method for formation of long range contacts is through the use of A-minor motifs, wherein an adenosine fits into the minor groove of a Watson:Crick base-pair (Nissen et al., 2001). There are four such motifs in our model (Figure 5A) between distant residues in the primary structure that have been evolutionarily maintained. These motifs likely play a significant role in reducing the energetic cost of bringing the parallel helices in close proximity by constructing a network of helix-helix interactions. For example, A88-G151-C33 affixes the J4/5 interhelical region near P2 while A117-G83-C57 appears to assist in coaxial organization of P3 and P4. The A71-G22-C163 motif links L4 to P2, which induces a near-continuous array of base stacking between P1, P2, L4, and L5 nucleotides (Figure 7C). Interestingly, this base stacking involves positions within the antiterminator sequence, suggesting that stacking energies are involved in the preferential sequestration of these nucleotides into P1 in response to Mg^{2+}, rather than the antiterminator helix. Finally, the A155-G107-C99 motif anchors P5 to P2 via the UAA/GAN motif and L5 residues (Lee et al., 2006).

Additional long-range base interactions occur within interhelical junctions that mediate sharp directional changes between adjacent helices or at the base of the molecule where antiterminator nucleotides, P2, L5, and L4 converge (Figure 7). For example, noncanonical pairings are present at the apex of the structure in a region between P6 and P2, facilitating the sharp angle between P2 and P3 helices. Near Mg3 in P2, the conserved U24 nucleobase forms a base-triple with G100 and A106 of L5. Additionally, an antiterminator nucleotide, U167, pairs to the Hoogsteen edge of A101 as well as the A103 Watson-Crick edge. Both of these interactions fasten L5 to the lower region of P2. An additional base-pair between A72 and A105 adds a direct contact between L4 and L5 and completes the network of P2-L5-L4 connections.

In total, our data indicate that the function of the M-box metalloregulatory RNA is to correlate intracellular Mg^{2+} with formation of terminator or antiterminator helices. The convergence of the long-range base interactions and A-minor motifs to the region of the structure that includes, or is adjacent to, Mg^{2+} and antiterminator nucleotides is likely to preferentially stabilize P1 rather than the mutually exclusive antiterminator helix. Specifically, in addition to Watson:Crick base pairing, certain antiterminator positions are sequestered into tertiary structure features in the Mg^{2+}-bound state, including base triples and base stacking within the tripartite structure formed by L4, L5, and P2. These observations reveal a simple, yet elegant mechanism for metal-mediated occlusion of antiterminator nucleotides. Consistent with this model, the positions that are most highly conserved for M-box RNAs are those that interact with metals and assist in coordinating the L4-L5-P2 tripartite structure (Figures 6, 7, S1, and S13). Therefore, the structural features exhibited by the *B. subtilis mgtE* aptamer domain are expected to be general features for the other members of the M-box riboswitch class.

DISCUSSION

In this work, we have described an RNA-based divalent cation sensor using a variety of in vivo and in vitro techniques. As such, a comparison to the previously characterized *Salmonella enterica* RNA, a proposed cation sensor, could highlight general rules for RNA-based metal sensors (Cromie et al., 2006). Unfortunately, as this RNA and M-box RNAs share no similarity at the primary or secondary structure level, a direct structural comparison is not particularly useful. The commonality between these two RNA classes reside in the fact that both appear to utilize a transcription attenuation-like genetic control mechanism through predicted Mg^{2+}-regulated switching between mutually exclusive helices. However, while the M-box RNAs described herein contain identifiable intrinsic terminator sequences, the novel mechanism by which helix switching in the *Salmonella enterica* RNA influences transcription is not fully resolved. Nonetheless, the presence of two distinct RNA elements utilized as metal sensors underscores the essential nature of metal ion homeostasis at all possible levels (i.e. RNA and protein) and raises the possibility of undiscovered RNA-based metal sensors. The data presented herein provide a structural and biochemical framework for comparative analyses of such metalloregulatory RNAs.

The M-box RNA structure is unique in many ways but is built upon principles observed previously for other RNAs. First, the regulatory RNA is remarkably similar in character to riboswitch RNAs, complete with a large evolutionarily conserved aptamer domain that controls formation of mutually exclusive terminator and antiterminator helices. Given the ease to which divalent metals interact with RNA polymers, it is reasonable to ask why such a large, highly conserved RNA structure would be required for metal sensing. The results of our biochemical and biophysical tests suggest that a potential explanation emanates from the cooperative binding of metal ligands. Where other riboswitch aptamer domains have evolved to bind a single ligand, the M-box RNA associates with multiple metal ion ligands and tertiary formation is highly cooperative, perhaps demanding the increased information content. This feature may also allow the RNA to sense small changes in Mg^{2+} concentration, thereby offering genetic control over a more narrow range than for noncooperative

(D) SHAPE probing with 5 mM Mg^{2+}, 5 mM Ca^{2+}, 5 mM Mn^{2+}, or in the absence of divalents revealed that multiple divalent metals could induce probing changes indicative of terminator formation (cf. Figure 3F). The extent of these probing changes is highlighted by the graph and the line traces.

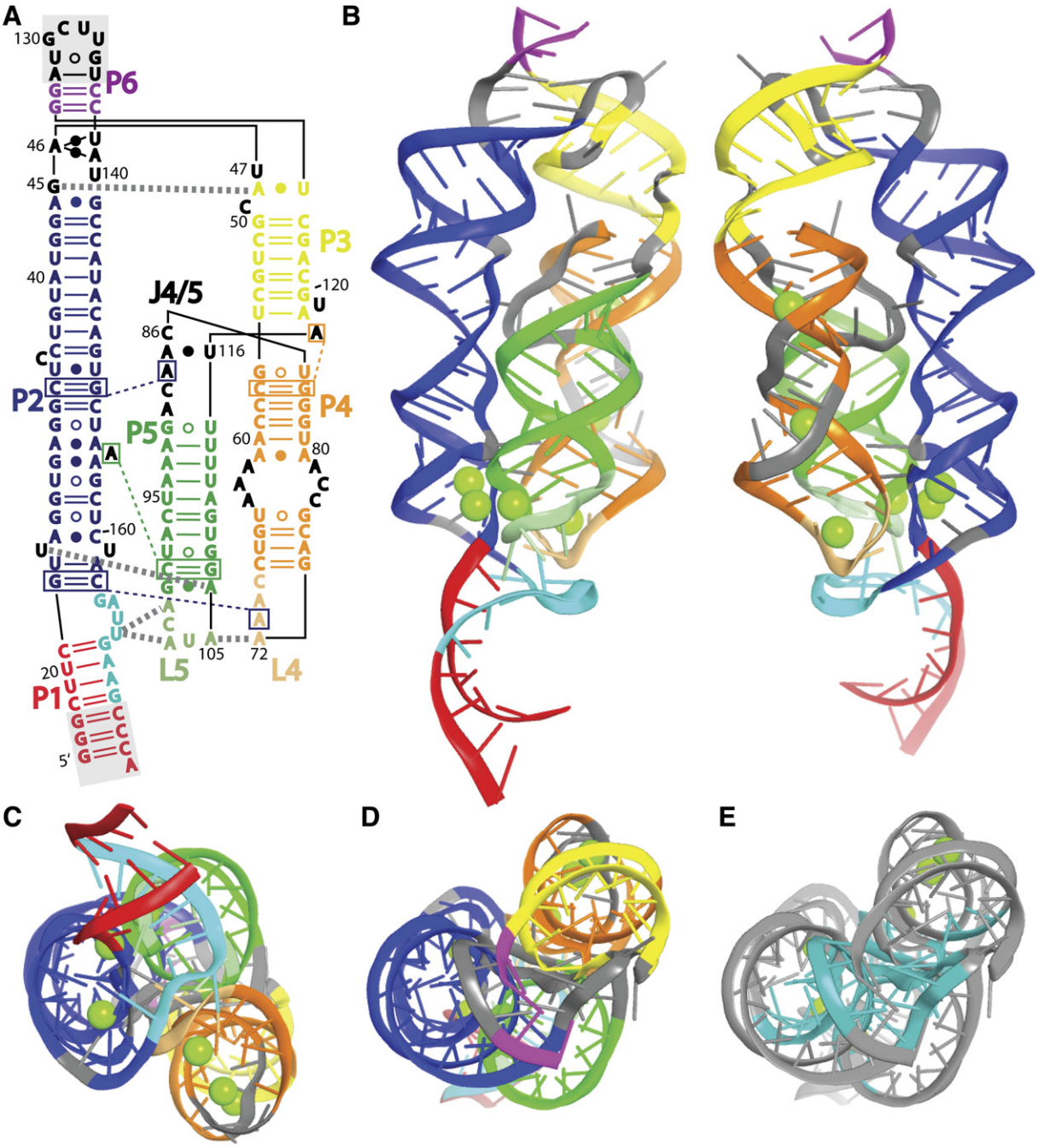

Figure 5. Global Architecture of an M-box RNA Bound to Mg^{2+}

(A) Secondary structure diagram based on the tertiary structure of *mgtE* aptamer domain is shown with the following color scheme: P1-red; P2-blue; P3-yellow; P4/L4-orange; P5/L5-green; P6-magenta; joining (J) regions-black; antiterminator-cyan. Open and closed circles mark G:U and noncanonical pairs, respectively. Long-range base pairs are connected by heavy dashed lines. Four A-minor motifs are boxed and connected by thin dashed lines. Gray shaded residues in P1 and P6 indicate positions that were added for crystallization and positions that are disordered in the structure, respectively.

(B) Two views of the aptamer domain model are shown with six Mg^{2+} depicted as green spheres. The second panel is rotated 180° about the *y* axis relative to the first panel. Colors are as in (A).

(C) A view of the structure rotated 90° about the *x* axis shows P1, the antiterminator, and the three parallel helices. Note the metal ions that decorate the tripartite interface around L4, L5, and P2.

(D) The image in (C) was rotated 180 about the *x* axis to show P6 atop P2, P5 and P3, which coaxially stacks on P4. Disordered residues (128–135) in P6 would connect the magenta strands on this face of the molecule.

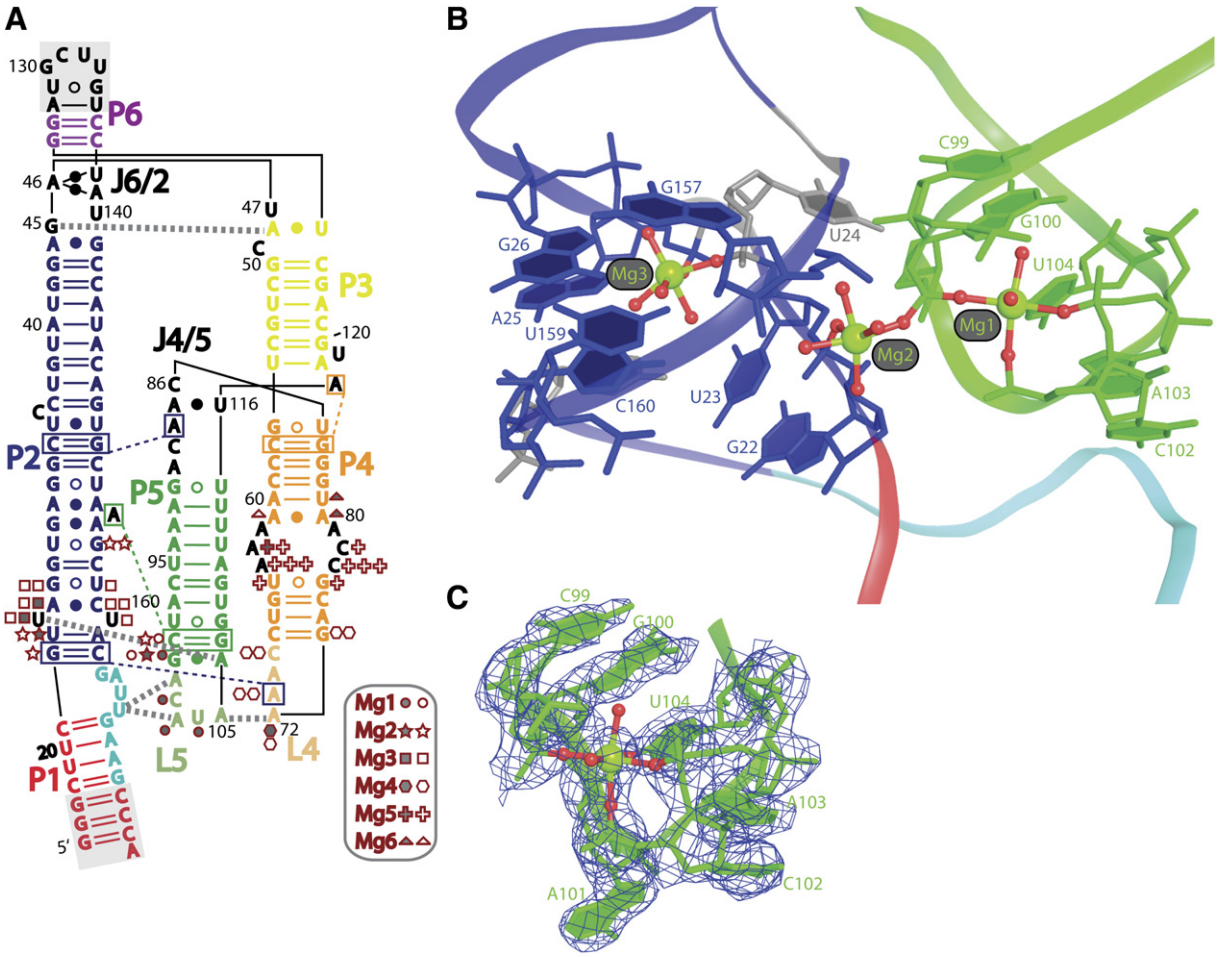

Figure 6. RNA-Metal Interactions

(A) Secondary structure shows the positions of inner- and outer-sphere contacts using shaded and open symbols, respectively, for the six Mg^{2+} coordinated to the RNA. Each Mg^{2+} has a unique symbol denoted in the legend. All other symbols and coloring are as in Figure 5A.

(B) Nucleotides that contact Mg1-3 via inner- and outer-sphere interactions are labeled and shown as sticks on a ribbon model of the phosphate backbone. P4 and L4, which would be located in the background of this image, have been omitted for clarity. A total of 4, 2, and 2 direct RNA oxygen atoms are coordinated to Mg1, Mg2, and Mg3, respectively. Only one of these RNA contacts (U104 O4) does not involve a nonbridging phosphate oxygen. Residue G100 is flanked by Mg1 and Mg2 coordinating to its two nonbridging phosphate oxygens. Residues that contact Mg1-3 cluster near the tripartite region of long-range tertiary contacts formed by L4, L5, and P2. Stereo views with electron density maps for all six Mg^{2+} sites are in Figure S11 and metal-RNA coordination distances are listed in Figure S10.

(C) The experimental electron density map contoured at 1.5 σ is shown for Mg1 and nucleotides contacted through inner- and outer-sphere interactions.

regulatory RNAs. Another key principle for RNA structures that the M-box employs is the use of Mg^{2+} to transition into a fully folded tertiary conformation (Draper et al., 2005; Sigel and Pyle, 2007; Woodson, 2005). However, two features of M-box RNAs render them as metal sensors rather than simply another structured RNA region. First, metal ions promote a compacted RNA tertiary structure for the explicit purpose of governing the accessibility of a short nucleotide tract. The availability of this signaling sequence can then be directly correlated to formation of terminator or antiterminator helices. Second, the apparent K_D for the metal-induced tertiary conformation is tuned to an appropriate intracellular concentration, thereby imparting sensory function to the overall structure. In fact, our data suggest that the *B. subtilis* M-box RNA is capable of responding to multiple divalent ions in vitro at millimolar concentrations (Figure 4). However, total metal ion concentrations reported for *E. coli*, which are likely to reflect those of *B. subtilis*, predict that Mg^{2+} is the only divalent ion present at a level sufficient to trigger the M-box

(E) Nucleotides that are protected based on hydroxyl radical footprinting in the presence of Mg^{2+} are highlighted in teal with other nucleotides shown in gray, showing a clear correlation between protected residues and the inner core of the RNA structure (See Figures 3A and 3F).

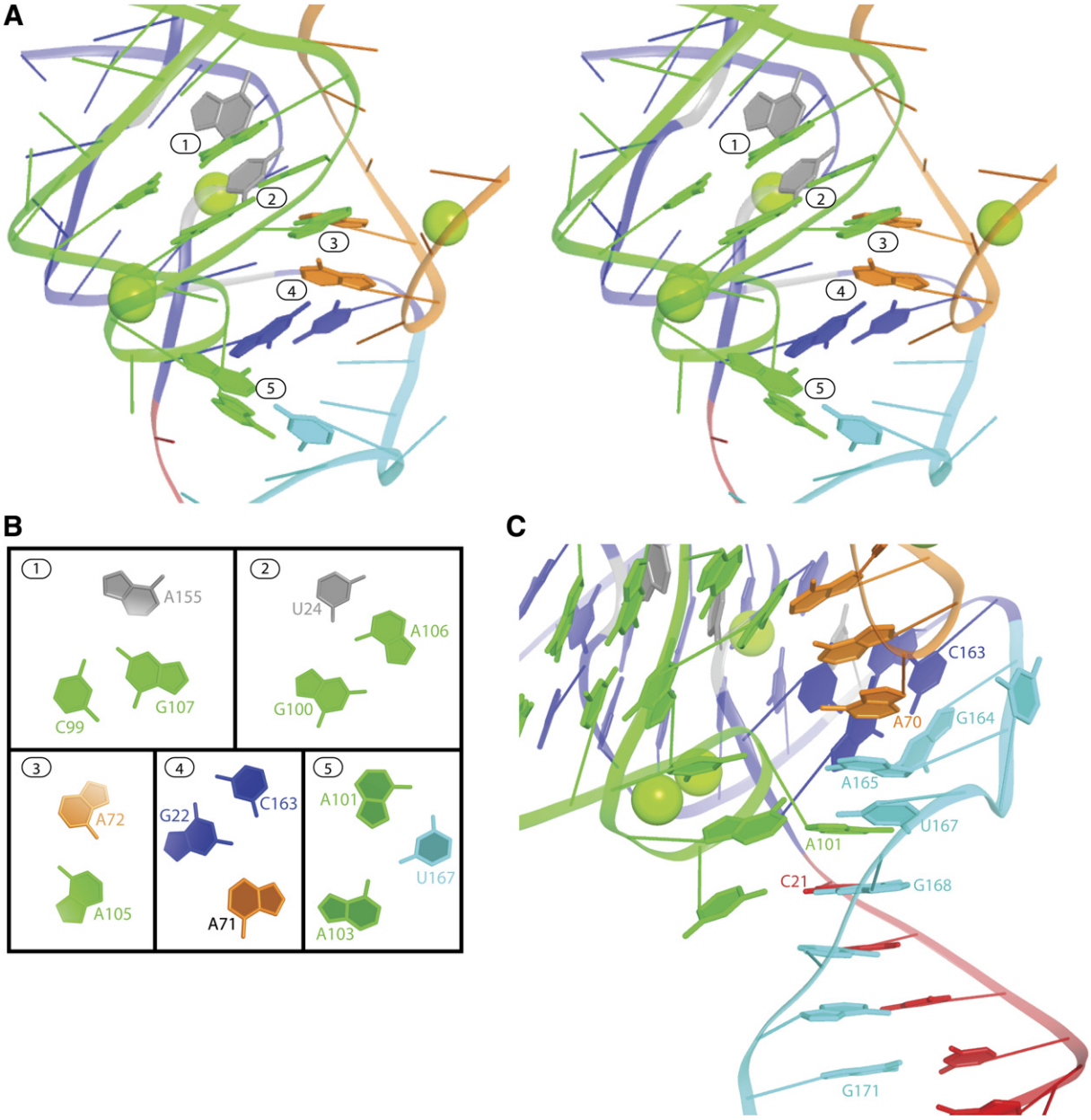

Figure 7. Sequestration of Antiterminator Nucleotides via Long-Range Base Interactions and Base Stacking

(A) A stereo view comprising the region of the molecule where P2, L5, L4, and antiterminator nucleotides converge is illustrated. Nucleotides involved in long-range base interactions are shown as filled bases on a ribbon model of the phosphate backbone. A total of five such interactions stabilize the region of the molecule adjacent to, or including, antiterminator nucleotides. Four canonical base pairs, involving G168–G171 as predicted from secondary structure, complete the sequestration of antiterminator positions. Color schemes match with Figure 5A.

(B) The base interactions numbered in (A) are presented individually from a top-down perspective.

(C) In addition to base interactions highlighted in (A) and (B), this region of the molecule is enriched in base stacking between P1, P2, L4, and L5 residues. These interactions are likely to be important in stabilizing the overall compacted tertiary conformation and for sequestration of antiterminator nucleotides (cyan).

riboswitch (Outten and O'Halloran, 2001). The total concentration of divalent ions other than Mg^{2+} are no greater than ~200 μM, with free (unbound) concentrations presumed to be substantially lower. Thus, while the *B. subtilis* M-box RNA is not specific for a particular divalent ion in vitro, Mg^{2+} is the only ion that the RNA is likely to respond to in vivo.

Based upon the insights provided by these studies on a metalloregulatory RNA, one could imagine similar elements may be used to selectively sense other metal ions.

In support of this idea, several M-box RNAs reside in the 5′ UTR of putative manganese transporters as well as uncharacterized transporters. Furthermore, two other orphan riboswitch classes are in part associated with genes that regulate metal ions. In total, the *B. subtilis mgtE* RNA aptamer may serve as a model for additional RNA-based metal sensors that are capable of regulating gene expression simply by tuning tertiary structure formation to a particular metal binding affinity.

EXPERIMENTAL PROCEDURES

DNA Oligonucleotides, Chemicals, Strains, and Plasmids

DNA oligonucleotides were purchased from Integrated DNA Technologies. Chemicals were purchased from Sigma. All strains were derived from IA40 (Bacillus Genetic Stock Center, Ohio). Fusions to *lacZ* were accomplished via pDG1661, which ectopically inserts into the nonessential *amyE* locus. Correct transformants were checked for chloramphenicol resistance (5 μg ml^{-1}) and spectinomycin sensitivity (100 μg ml^{-1}). In order to construct the *mgtE-lacZ* fusion, nucleotides −486 to + 25 relative to the *mgtE* translational start were cloned into pDG1661 via restriction sites added to oligonucleotide primers. Nucleotides −487 to −143 and −487 to −235 were cloned into pDG1661 for construction of promoter-*lacZ* and aptamer-*lacZ* fusions, respectively. Mutations were introduced using the QuikChange mutagenesis protocol (Strategene) and were verified by DNA sequencing. DNA was transformed as described (Jarmer et al., 2002).

Growth Conditions

In general, cells were incubated at 37°C in glucose minimal medium [0.5% glucose, 0.5 mM $CaCl_2$, 5 μM $MnCl_2$, 15 mM $(NH_4)_2SO_4$, 80 mM K_2HPO_4, 44 mM KH_2PO_4, 3.9 mM sodium citrate, and 50 μg ml^{-1} amino acids (tryptophan, methionine, lysine)]. $MgCl_2$ was added as defined in text. Cultures containing 2.5 mM $MgCl_2$ were grown at 37°C overnight, without shaking. The following day, cells were incubated while shaking, cultured to mid-exponential growth phase, pelleted (t_0), washed twice in medium lacking Mg^{2+}, and resuspended to a final OD_{600} of 0.1. $MgCl_2$ was added to 5 μM or 2.5 mM for "low" or "high" conditions, respectively, prior to incubation again at 37°C. At $t_{5.5}$ (hours), cells were harvested for analysis. Growth of manganese-limited cells was achieved similarly except that 2.5 mM $MgCl_2$ was maintained throughout the experimentation and at OD_{600} = 0.1 $MnCl_2$ was either eliminated or added at 5 μM for "low" and "high" conditions, respectively. For control of iron levels, either 5 μM $FeCl_2$ or 100 μM of the iron chelator 2,2′-dipyridyl (Biachoo et al., 2002) was added to cultures at OD_{600} = 0.1 to generate "high" or "low" iron conditions, respectively. For assays involving limitation of all divalents, cell pellets were resuspended in glucose minimal medium lacking $MgCl_2$, $CaCl_2$, and $MnCl_2$. Each divalent was individually added to cultures at a concentration of 50 μM. Measurements of β-galactosidase activity are detailed in the Supplementary Materials.

RNA Structural Probing and Transcription Termination Assays

Hydroxyl radical footprinting, SHAPE, and in-line probing techniques as well as assays of Mg^{2+}-induced termination in vitro are detailed in the Supplemental Data.

Analytical Ultracentrifugation and RNA Size-Exclusion Chromatography

Measurements of Mg^{2+}-induced changes in hydrodynamic radius assayed by AUC and size-exclusion chromatography are described in detail within the Supplemental Data.

Structure Determination

The estimate for coordinate error in the model based on R_{free} is 0.26 Å calculated using the Cruickshank DPI method implemented in the program Refmac5. Details for RNA production to structure determination are included in Supplemental Data.

Supplemental Data

Supplemental Data include Supplemental Experimental Procedures, Supplemental References, thirteen figures, and one table and can be found with this article online at http://www.cell.com/cgi/content/full/130/5/878/DC1/.

ACKNOWLEDGMENTS

We thank Chad Brautigam for assistance with AUC, Alexis Kertsburg for assisting with milligram-scale RNA production, Jennifer A. Collins for construction of the *mgtE-lacZ* transcriptional fusion, and Ronald Breaker, Ali Nahvi, Matthew Porteus, and J. K. Wickiser for reading drafts of the manuscript. We are indebted to Robert Batey for offering comments on the crystallographic data and manuscript. This research was funded by the Searle Scholars Program, the UT Southwestern Medical Center Endowed Scholars Program, and the Welch Foundation. Funding for C.D. was supplied by the Sara and Frank McKnight Fund for Biochemical Research.

Results shown in this report are derived from work performed at Argonne National Laboratory, Structural Biology Center Beamline 19ID at the Advanced Photon Source with assistance from N.A.C. Duke. Argonne is operated by UChicago Argonne, LLC, for the U.S. Department of Energy, Office of Biological and Environmental Research under contract DE-AC02-06CH11357.

Received: March 8, 2007
Revised: May 24, 2007
Accepted: June 27, 2007
Published: September 6, 2007

REFERENCES

Barrick, J.E., Corbino, K.A., Winkler, W.C., Nahvi, A., Mandal, M., Collins, J., Lee, M., Roth, A., Sudarsan, N., Jona, I., et al. (2004). New RNA motifs suggest an expanded scope for riboswitches in bacterial genetic control. Proc. Natl. Acad. Sci. USA *101*, 6421–6426.

Batey, R.T. (2006). Structures of regulatory elements in mRNAs. Curr. Opin. Struct. Biol. *16*, 299–306.

Biachoo, N., Wang, T., Ye, R., and Helmann, J.D. (2002). Global analysis of the Bacillus subtilis Fur regulon and the iron starvation stimulon. Mol. Microbiol. *6*, 1613–1629.

Cate, J.H., Hanna, R.L., and Doudna, J.A. (1997). A magnesium ion core at the heart of a ribozyme domain. Nat. Struct. Biol. *4*, 553–558.

Corbino, K.A., Barrick, J.E., Lim, J., Welz, R., Tucker, B.J., Puskarz, I., Mandal, M., Rudnick, N.D., and Breaker, R.R. (2005). Evidence for a second class of *S*-adenosylmethionine riboswitches and other regulatory RNA motifs in alpha-proteobacteria. Genome Biol. *6*, R70.

Cowan, J.A. (1993). Metallobiochemistry of RNA. $Co(NH_3)_6^{3+}$ as a probe for Mg^{2+} (aq) binding sites. J. Inorg. Biochem. *49*, 171–175.

Cromie, M.J., Shi, Y., Latifi, T., and Groisman, E.A. (2006). An RNA sensor for intracellular Mg^{2+}. Cell *125*, 71–84.

Das, R., Travers, K.J., Bai, Y., and Herschlag, D. (2005). Determining the Mg^{2+} stoichiometry for folding an RNA metal ion core. J. Am. Chem. Soc. *127*, 8272–8273.

de Hoon, M.J., Makita, Y., Nakai, K., and Miyano, S. (2005). Prediction of transcriptional terminators in *Bacillus subtilis* and related species. PLoS Comput. Biol. *1*, e25. 10.1371/journal.pcbi.0010025.

DeRose, V.J. (2003). Metal ion binding to catalytic RNA molecules. Curr. Opin. Struct. Biol. *13*, 317–324.

Draper, D.E., Grilley, D., and Soto, A.M. (2005). Ions and RNA folding. Annu. Rev. Biophys. Biomol. Struct. *34*, 221–243.

Gardner, R.C. (2003). Genes for Mg^{2+} transport. Curr. Opin. Plant Biol. *6*, 263–267.

Griffiths-Jones, S., Moxon, S., Marshall, M., Khanna, A., Eddy, S.R., and Bateman, A. (2005). Rfam: annotating noncoding RNAs in complete genomes. Nucleic Acids Res. *33*, D121–D124.

Gusarov, I., and Nudler, E. (1999). The mechanism of intrinsic transcription termination. Mol. Cell *3*, 495–504.

Hmiel, S.P., Snavely, M.D., Miller, C.G., and Maguire, M.E. (1986). Magnesium transport in *Salmonella typhimurium*: Characterization of magnesium influx and cloning of a transport gene. J. Bacteriol. *168*, 1444–1450.

Hougland, J.L., Kravchuk, A.V., Herschlag, D., and Piccirilli, J.A. (2005). Functional identification of catalytic metal ion binding sites within RNA. PLoS Biol. *3*, e277. 10.1371/journal.pbio.0030277.

Jarmer, H., Berka, R., Knudsen, S., and Saxild, H.H. (2002). Transcriptome analysis documents induced competence of *Bacillus subtilis* during nitrogen limiting conditions. FEMS Microbiol. Lett. *206*, 197–200.

Kehres, D.G., and Maguire, M.E. (2002). Structure, properties and regulation of magnesium transport proteins. Biometals *15*, 261–270.

Klein, D.J., Moore, P.B., and Steitz, T.A. (2004). The contribution of metal ions to the structural stability of the large ribosomal subunit. RNA *10*, 1366–1379.

Landick, R., and Yanofsky, C. (1987). Transcription attenuation. In *Escherichia coli* and *Salmonella typhimurium*: Cellular and Molecular Biology, F.C. Neidhardt, ed. (Washington, D.C.: American Society for Microbiology), pp. 1276–1301.

Latham, J.A., and Cech, T.R. (1989). Defining the inside and outside of a catalytic RNA molecule. Science *245*, 276–282.

Lee, J.C., Gutell, R.R., and Russell, R. (2006). The UAA/GAN internal loop motif: a new RNA structural element that forms a cross-strand AAA stack and long-range tertiary interactions. J. Mol. Biol. *360*, 978–988.

Li, Y., and Breaker, R.R. (1999). Kinetics of RNA degradation by specific base catalysis of transesterification involving the 2′-hydroxyl group. J. Am. Chem. Soc. *121*, 5364–5372.

Macdiarmid, C.W., and Gardner, R.C. (1998). Overexpression of the *Saccharomyces cerevisiae* magnesium transport system confers resistance to aluminum ions. J. Biol. Chem. *273*, 1727–1732.

Maguire, M.E. (2006). Magnesium transporters: properties, regulation and structure. Front. Biosci. *111*, 3149–3163.

Merino, E.J., Wilkinson, K.A., Coughlan, J.L., and Weeks, K.M. (2005). RNA structure analysis at single nucleotide resolution by selective 2′-hydroxyl acylation and primer extension (SHAPE). J. Am. Chem. Soc. *127*, 4223–4231.

Mironov, A.S., Gusarov, I., Rafikov, R., Lopez, L.E., Shatalin, K., Kreneva, R.A., Perumov, D.A., and Nudler, E. (2002). Sensing small molecules by nascent RNA: a mechanism to control transcription in bacteria. Cell *111*, 747–756.

Moore, C.M., and Helmann, J.D. (2005). Metal ion homeostasis in *Bacillus subtilis*. Curr. Opin. Microbiol. *8*, 188–195.

Nissen, P., Ippolito, J.A., Ban, N., Moore, P.B., and Steitz, T.A. (2001). RNA tertiary interactions to the large ribosomal subunit: the A-minor motif. Proc. Natl. Acad. Sci. USA *98*, 4899–4903.

Outten, C.E., and O'Halloran, T.V. (2001). Femtomolar sensitivity of metalloregulatory proteins controlling zinc homeostasis. Science *292*, 2488–2492.

Pennella, M.A., and Giedroc, D.P. (2005). Structural determinants of metal selectivity in prokaryotic metal-responsive transcriptional regulators. Biometals *18*, 413–428.

Selmer, M., Dunham, C.M., Murphy, F.V., 4th, Weixlbaumer, A., Petry, S., Kelley, A.C., Weir, J.R., and Ramakrishnan, V. (2006). Structure of the 70S ribosome complexed with mRNA and tRNA. Science *313*, 1935–1942.

Serganov, A., Polonskaia, A., Phan, A.T., Breaker, R.R., and Patel, D.J. (2006). Structural basis for gene regulation by a thiamine pyrophosphate-sensing riboswitch. Nature *441*, 1167–1171.

Sigel, R.K., and Pyle, A.M. (2007). Alternative roles for metal ions in enzyme catalysis and the implications for ribozyme chemistry. Chem. Rev. *107*, 97–113.

Smith, R.L., and Maguire, M.E. (1995). Distribution of the CorA Mg^{2+} transport system in Gram-negative bacteria. J. Bacteriol. *177*, 1638–1640.

Smith, R.L., and Maguire, M.E. (1998). Microbial magnesium transport: unusual transporters searching for identity. Mol. Microbiol. *28*, 217–226.

Soukup, G.A., and Breaker, R.R. (1999). Relationship between internucleotide linkage geometry and the stability of RNA. RNA *5*, 1308–1325.

Takamoto, K., Das, R., He, Q., Doniach, S., Brenowitz, M., Herschlag, D., and Chance, M.R. (2004). Principles of RNA compaction: insights from the equilibrium folding pathway of the P4–P6 RNA domain in monovalent cations. J. Mol. Biol. *343*, 1195–1206.

Vicens, Q., and Cech, T.R. (2006). Atomic level architecture of group I introns revealed. Trends Biochem. Sci. *31*, 41–51.

Winkler, W.C. (2005a). Riboswitches and the role of noncoding RNA in bacterial metabolic control. Curr. Opin. Chem. Biol. *9*, 594–602.

Winkler, W.C. (2005b). Metabolic monitoring by bacterial mRNAs. Arch. Microbiol. *183*, 151–159.

Winkler, W.C., and Breaker, R.R. (2005). Regulation of bacterial gene expression by riboswitches. Annu. Rev. Microbiol. *59*, 487–517.

Winkler, W.C., Nahvi, A., and Breaker, R.R. (2002). Thiamine derivatives bind messenger RNAs directly to regulate bacterial gene expression. Nature *419*, 952–956.

Winkler, W.C., Nahvi, A., Roth, A., Collins, J.A., and Breaker, R.R. (2004). Control of gene expression by a natural metabolite-responsive ribozyme. Nature *428*, 281–286.

Winkler, W.C., Nahvi, A., Sudarsan, N., Barrick, J.E., and Breaker, R.R. (2003). An mRNA structure that controls gene expression by binding *S*-adenosylmethionine. Nat. Struct. Biol. *10*, 701–707.

Woodson, S.A. (2005). Metal ions and RNA folding: a highly charged topic with a dynamic future. Curr. Opin. Chem. Biol. *9*, 104–109.

Accession Numbers

Structural coordinates have been deposited in the RCSB Protein Data Bank with accession code 2QBZ.